Centrosome repositioning in T cells is biphasic and driven by microtubule end-on capture-shrinkage

Jason Yi,[1] Xufeng Wu,[1] Andrew H. Chung,[2] James K. Chen,[2] Tarun M. Kapoor,[3] and John A. Hammer[1]

[1]Cell Biology and Physiology Center, National Heart, Lung, and Blood Institute (NHLBI), National Institutes of Health (NIH), Bethesda, MD 20892
[2]Department of Chemical and Systems Biology, Stanford University School of Medicine, Stanford, CA 94305
[3]Laboratory of Chemistry and Cell Biology, The Rockefeller University, New York, NY 10065

T cells rapidly reposition their centrosome to the center of the immunological synapse (IS) to drive polarized secretion in the direction of the bound target cell. Using an optical trap for spatial and temporal control over target presentation, we show that centrosome repositioning in Jurkat T cells exhibited kinetically distinct polarization and docking phases and required calcium flux and signaling through both the T cell receptor and integrin to be robust. In "frustrated" conjugates where the centrosome is stuck behind the nucleus, the center of the IS invaginated dramatically to approach the centrosome. Consistently, imaging of microtubules during normal repositioning revealed a microtubule end-on capture-shrinkage mechanism operating at the center of the IS. In agreement with this mechanism, centrosome repositioning was impaired by inhibiting microtubule depolymerization or dynein. We conclude that dynein drives centrosome repositioning in T cells via microtubule end-on capture-shrinkage operating at the center of the IS and not cortical sliding at the IS periphery, as previously thought.

Introduction

The repositioning of the centrosome or spindle pole relative to the cell cortex is required for numerous fundamental biological processes, including polarized secretion and the asymmetric division of eggs and stem cells (Grill and Hyman, 2005; Gönczy, 2008; Li and Gundersen, 2008). Central to a few well-studied examples is the presence in the cell cortex of the microtubule minus end–directed motor cytoplasmic dynein, which repositions the centrosome/spindle pole by pulling on a subset of interphase/astral microtubules that contact the cortex. Pulling can occur via either of two mechanisms. In the cortical sliding mechanism, dynein's efforts to walk to the minus end of the microtubule at the centrosome while simultaneously being held in place at the cortex results in the microtubule sliding past dynein so as to reel the centrosome in. The best example of this mechanism is in budding yeast during anaphase, where dynein anchored in the bud cortex pulls the nucleus/mitotic spindle into the mother-bud neck by pulling on astral microtubules emanating from the budward-directed spindle pole (Moore and Cooper, 2010). In the second mechanism, cortically bound dynein interacts with the plus end of a microtubule in end-on fashion in such a way as to couple the subsequent depolymerization of the microtubule with the movement of the centrosome toward the cortex. This capture-shrinkage mechanism, which likely harnesses both dynein's power stroke and the force of microtubule depolymerization to drive centrosome repositioning, has been demonstrated recently in vitro (Laan et al., 2012), and probably drives asymmetric spindle positioning in single-cell *Caenorhabditis elegans* embryos (Nguyen-Ngoc et al., 2007). This mechanism may also facilitate spindle pole body positioning in budding yeast before mitosis (Ten Hoopen et al., 2012).

A dramatic example of centrosome positioning in vertebrate cells occurs in T lymphocytes immediately after the recognition by the T cell of stimulatory antigen presented on the surface of an antigen-presenting cell (APC; Huse, 2012; Angus and Griffiths, 2013). The principal consequence of this recognition, the focused secretion of effector molecules in the direction of the bound APC, is orchestrated by a series of rapid, synchronous, large-scale polarization events within the T cell that involve major rearrangements of its actin and microtubule cytoskeletons. These rearrangements result in the rapid formation of an organized junction between the T cell and the APC known as

Correspondence to John A. Hammer: hammerj@nhlbi.nih.gov

Abbreviations used in this paper: APC, antigen-presenting cell; IS, immunological synapse; MTOC, microtubule-organizing center; SEE, staphylococcal enterotoxin E; TCR, T cell receptor; WT, wild type.

The Rockefeller University Press $30.00
J. Cell Biol. Vol. 202 No. 5 779–792
www.jcb.org/cgi/doi/10.1083/jcb.201301004

the immunological synapse (IS), in which the T cell's cortical actin cytoskeleton, adhesion molecules, and T cell receptor (TCR) microclusters are organized in radial symmetric zones facing the APC (Choudhuri and Dustin, 2010). At approximately the same time, the T cell's centrosome or microtubule-organizing center (MTOC) moves to a position that is just underneath the plasma membrane at the center of the IS (Geiger et al., 1982; Kupfer et al., 1983; Stinchcombe et al., 2006). This rapid and robust repositioning of the T cell's MTOC allows the microtubule minus end–directed transport of vesicles containing effector molecules (e.g., cytokines or lytic molecules) to be directed toward and terminated immediately adjacent to the bound APC for subsequent polarized secretion.

Previous work has shed light on several aspects of MTOC repositioning in T cells. With regard to triggering stimuli, repositioning appears to require key mediators of TCR-dependent signaling (Lck/Fyn, ZAP-70, Slp-76, and LAT; Lowin-Kropf et al., 1998; Blanchard et al., 2002; Kuhné et al., 2003; Martín-Cófreces et al., 2006; Tsun et al., 2011), as well as DAG-dependent activation of PKC (Quann et al., 2009, 2011), but not the T cell's major integrin LFA-1 (Combs et al., 2006) or the normal rise in intracellular calcium concentration that occurs upon TCR engagement (Quann et al., 2009). As for the motive force, repositioning appears to require dynein, as the process is completely blocked by RNAi-mediated knockdown of the dynein heavy chain, as well as by overexpression of dynamitin, an inhibitor of the dynein regulator dynactin (Martín-Cófreces et al., 2008). Consistently, a GFP-tagged dynein subunit accumulates at the IS after DAG formation (Quann et al., 2009), and endogenous dynein concentrates at the IS periphery (Combs et al., 2006; although see Hashimoto-Tane et al., 2011). With regard to the underlying mechanism, the movement of the T cell's microtubule cytoskeleton after contact with an APC, as visualized using polarization light microscopy, together with images of fixed, end-stage T cell–APC conjugates stained for microtubules, suggests that repositioning is driven by the cortical sliding mechanism involving dynein anchored at the IS cortex (Kuhn and Poenie, 2002).

A major challenge in studying centrosome repositioning in T cells is that the process is extremely fast, going to completion within several minutes after APC contact. For this reason, most previous studies have used a static approach in which the T cell and APC are mixed together, incubated for 10–30 min, fixed, and scored for the percentage of centrosomes that are close to the IS. Besides providing no dynamic information, this approach yields high levels (~30%) of background repositioning because T cell–APC interaction is stochastic. One exception is the recent work from Huse and colleagues, who use the focused activation of a photo-activatable peptide–MHC complex bound to a glass surface to provide spatial and temporal control over MTOC repositioning (Quann et al., 2009). This approach does, however, suffer from the fact that the engaging entity is a glass surface, which precludes IS maturation. In this study, therefore, we used an optical trap to place an APC such that its initial point of contact with the T cell is exactly opposite from the location of the T cell's centrosome. In this way, the complete process of MTOC repositioning within the T cell could be dynamically imaged in quantitative fashion in the context of a T cell–APC conjugate, where IS maturation can occur. Using this and other tools, we reach different conclusions regarding several published aspects of centrosome repositioning in T cells, most notably regarding the underlying mechanism of this dynein-dependent process.

Results

Optical trap–controlled APC presentation induces robust MTOC repositioning in Jurkat T cells

To dynamically image and quantitate the complete process of centrosome repositioning within APC-engaged Jurkat T cells, we used a simple optical trap attached to a spinning disc confocal microscope to provide both temporal and spatial control over the presentation of the APC to the T cell. Specifically, we used the trap to place a staphylococcal enterotoxin E (SEE)–coated Raji B cell (the APC) adjacent to a coverslip-bound Jurkat T cell such that the Raji cell's initial point of contact with the surface of the T cell is exactly opposite from the position of the T cell's centrosome, marked by GFP-tagged centrin [cen]-2 or RFP-tagged pericentrin (Fig. 1 A). This method of controlling T cell engagement resulted in the rapid activation of TCR signaling, as evidenced by SEE-dependent calcium flux (Fig. 1, B and C), and resulted routinely in the rapid and robust repositioning of the T cell's MTOC to the site of contact with the Raji cell (Fig. 1 D; Video 1).

Fig. 2 A shows the scoring system used to categorize MTOC repositioning events (unless indicated otherwise, all scores were assigned 10 min after initial APC contact). Centrosomes that ended up >4 µm distant from the plane of contact, between 2 to 4 µm distant from the plane of contact, or <2 µm distant from the plane of contact were scored as "no repositioning", "partial repositioning", and "full repositioning", respectively. In addition, the Raji B cell sometimes repositions to the location of the Jurkat's MTOC ("APC repositioning"). We consider APC repositioning to be mechanistically equivalent to full repositioning. Fig. 2 B shows that MTOC repositioning in our trap-based assay is very robust, as 71.2% of Jurkat cells fully repositioned their MTOC after +SEE Raji engagement (WT +SEE). Including APC repositioning events in the category of full repositioning raises this value to 87.6%. Of note, partial repositioning events are very rare (4.1%), indicating that once centrosome repositioning is initiated, it almost always goes to completion. Events scored as no repositioning (8.2% of the total) are very interesting and are discussed below (see Fig. 4). Importantly, and in striking contrast to previous static assays where T cell–APC conjugation is stochastic, background MTOC repositioning was almost completely eliminated, as JCAM2.5 Jurkat cells, which lack the adaptor protein LAT critical for both TCR and LFA-1 signaling (Choudhuri and Dustin, 2010), exhibited only 5% full repositioning events (Fig. 2 B; JCAM2.5 +SEE).

TCR- and LFA-1–dependent signaling pathways and calcium are all required for robust MTOC repositioning

Previous studies using static assays have argued that MTOC repositioning in T cells requires signaling downstream from the

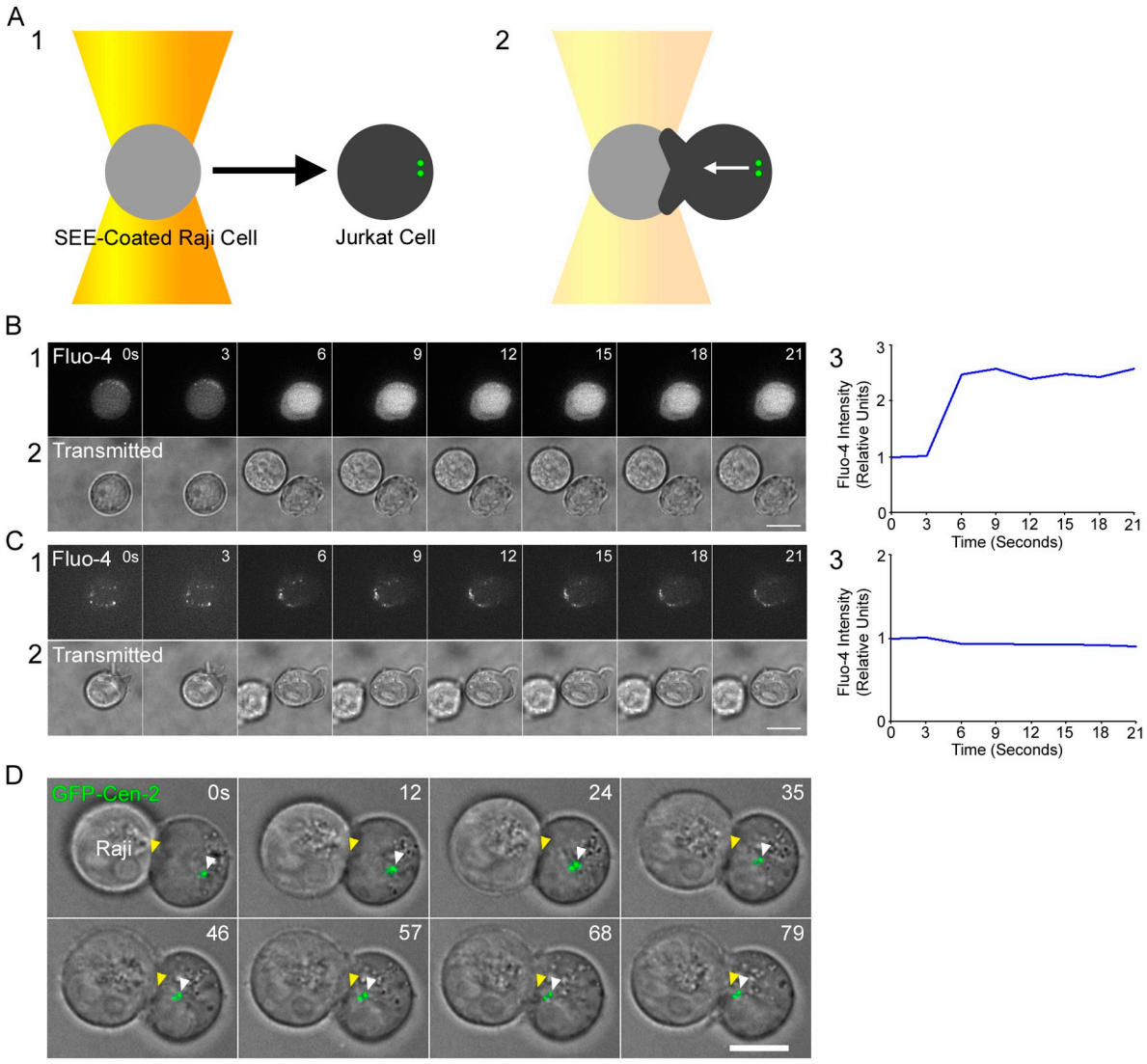

Figure 1. **Optical trap–based system for quantitating MTOC repositioning in Jurkat–APC conjugates.** (A) Cartoon showing the optical trap–controlled presentation of a SEE-coated Raji cell to a centrosome-marked Jurkat T cell (A1) resulting in MTOC repositioning to the site of contact (A2). Note that the MTOC in unengaged T cells is typically near the cell edge because the nucleus fills most of the cell's volume. (B and C) Jurkats conjugated to SEE-coated Raji cells (B) but not uncoated Raji cells (C) exhibit robust calcium flux immediately after optical trap–controlled contact (B1 and C1, Fluo-4AM signals; B2 and C2, transmitted images; B3 and C3, total cellular Fluo-4AM signals after contact with the Raji cell). (D) MTOC repositioning in a representative Jurkat immediately after optical trap–controlled engagement with a SEE-coated Raji cell (follow the yellow [IS] and white [green MTOC] arrowheads; see also Video 1). Bars, 10 µm.

TCR (Tsun et al., 2011) but not downstream from the T cell integrin LFA-1 (Combs et al., 2006). To estimate the individual contribution of TCR-dependent signaling to MTOC repositioning, we compared Jurkats conjugated to +SEE Raji cells (i.e., with TCR signaling) to Jurkats conjugated to −SEE Raji cells (i.e., without TCR signaling). From the data in Fig. 2 B (compare WT +SEE with WT −SEE) it is clear that although TCR signaling is required for robust MTOC repositioning, signaling through LFA-1 (and other co-stimulatory receptors) can result in measurable levels of MTOC repositioning. To estimate the individual contribution of LFA-1–dependent signaling to MTOC repositioning, we compared wild-type (WT) Jurkats (i.e., with LFA-1 signaling) to the LFA-1–deficient Jurkat cell line JB2.7 (i.e., without LFA-1 signaling). From the data in Fig. 2 B (compare WT +SEE with JB2.7 +SEE) it is clear that although LFA-1–dependent signaling is required for robust MTOC repositioning, signaling through the TCR (and other co-stimulatory receptors) can result in measurable levels of MTOC repositioning. Of note, transfection of the JB2.7 cell line with GFP-LFA-1α largely rescued the defect in MTOC polarization (see JB2.7 +SEE +LFA-1). Finally, conjugation of JB2.7 Jurkat cells with −SEE Raji cells (i.e., no TCR or LFA-1 signaling) resulted in the complete inhibition of APC/full repositioning (Fig. 2 B, JB2.7 −SEE). Together, these results indicate that, in contrast to a previous study (Combs et al., 2006), both TCR- and LFA-1–dependent signaling pathways are required for robust MTOC polarization in T cells.

We also note an interesting aspect of the results using JB2.7 Jurkats, which lack LFA-1–dependent adhesion as well as signaling. Specifically, in those repositioning events where

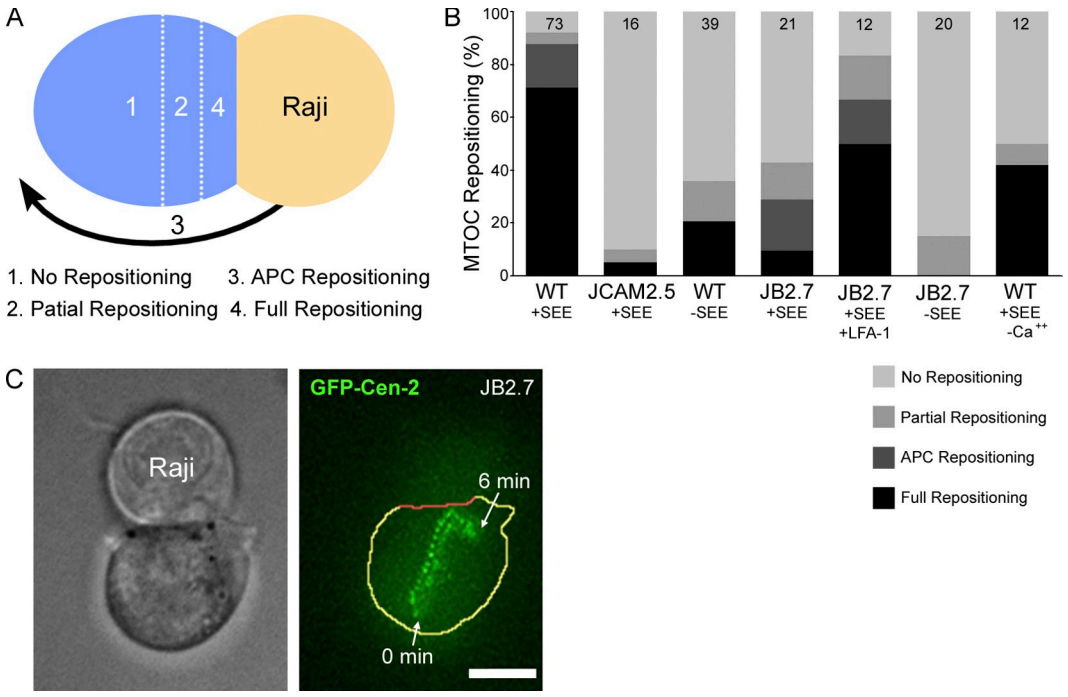

Figure 2. **Roles of TCR- and LFA-1-dependent signaling and calcium flux in MTOC repositioning.** (A) Grading system used in the MTOC repositioning assay. (B) Shown are the percent contributions of the four classes of MTOC repositioning for the indicated conjugates (see text). The *n* values are shown here and in following figures within the bar graph. (C) Bright-field image of a JB2.7 (LFA-1 minus) Jurkat engaged to a +SEE Raji cell (left) and a maximum projection over time of the GFP-Cen-2 signal in the JB2.7 cell (right; the JB2.7 cell is outlined in yellow except for its interface with the APC, which is in red). Bar, 10 µm.

the MTOC did undergo full repositioning, stacked images of the centrosome show that after reaching the IS it drifts away from the center of the IS (Fig. 2 C). This observation argues that tight adhesion between the T cell and the APC is required to stably position the MTOC at the center of the IS, as well as to augment its movement to the IS.

Finally, with regard to the two major consequences of PLC activation downstream of TCR ligation, it was recently reported that while the DAG-dependent activation of PKC is required for MTOC repositioning, the IP3-mediated rise in intracellular calcium is not (Quann et al., 2009). In contrast, we observe a very significant impairment in MTOC repositioning when both intracellular and extracellular calcium are effectively chelated (Fig. 2 B; compare WT +SEE $-Ca^{2+}$ with WT +SEE).

MTOC repositioning is biphasic

Previous studies have concluded that MTOC repositioning in T cells occurs at a single speed (3.6 ± 1.1 µm/min, Kuhn and Poenie, 2002; ∼3 µm/min, Quann et al., 2009). To characterize in detail the kinetics of MTOC repositioning, we labeled Jurkats with farnesylated RFP as well as with GFP-Cen-2 so that the approach of the MTOC to the plasma membrane at the IS could be gauged accurately. Typical repositioning events (Fig. 3 A; Video 2) suggested that this process actually occurs in two phases: relatively fast movement of the MTOC across most of the T cell's volume (referred to hereafter as the polarization phase), followed by slower movement of the MTOC as it approaches the IS (the docking phase). The transition between these two phases occurred in this example when the centrosome reached a distance of ∼2 µm from the synaptic membrane (Fig. 3 A, yellow arrowhead). Importantly, the docking phase leads to the close approximation of the centrosome to the plasma membrane at the IS (Fig. 3 A, white arrowhead), as reported previously using other methods (Stinchcombe et al., 2006). Stack overlays of typical full repositioning events (Fig. 3 B) reveal these two kinetic phases as an abrupt decrease in the spacing between successive centrosome spots once the centrosome gets within ∼2 µm of the IS (yellow arrowhead). Stack overlays also reveal a slight but reproducible change in the direction of the MTOC's movement relative to the plane of the IS as the MTOC transitions into the docking phase (Fig. 3 B). This direction change is likely due to the fact that the MTOC must navigate around the T cell's nucleus, which fills much of the T cell's total volume, during the polarization phase, but not during the docking phase (Fig. 3 C).

MTOC behavior that is similar to Fig. 3 A was obtained for eight additional Jurkat–APC conjugates possessing a fluorescently marked IS (Fig. 3 D). To better define the two phases, their average speeds, and the transition point between them, we determined the instantaneous speed of the MTOC at every time point in all nine repositioning events (Fig. 3, A and D) and plotted the values as a function of distance from the IS (Fig. 3 E). Assuming that repositioning is biphasic, we then fit the scatter plot to two clusters using cluster analysis by K means. The fitting yielded two distinct clusters with average speeds of 3.26 ± 0.77 µm/min and 0.9 ± 0.16 µm/min (Fig. 3 F; $P < 0.001$), which correspond to the polarization (green circles) and docking (red circles) phases, respectively, and indicated that the transition point between the two phases occurs 2.2 ± 0.3 µm from the IS (Fig. 3 E; see also Materials and methods). Critically, fitting to

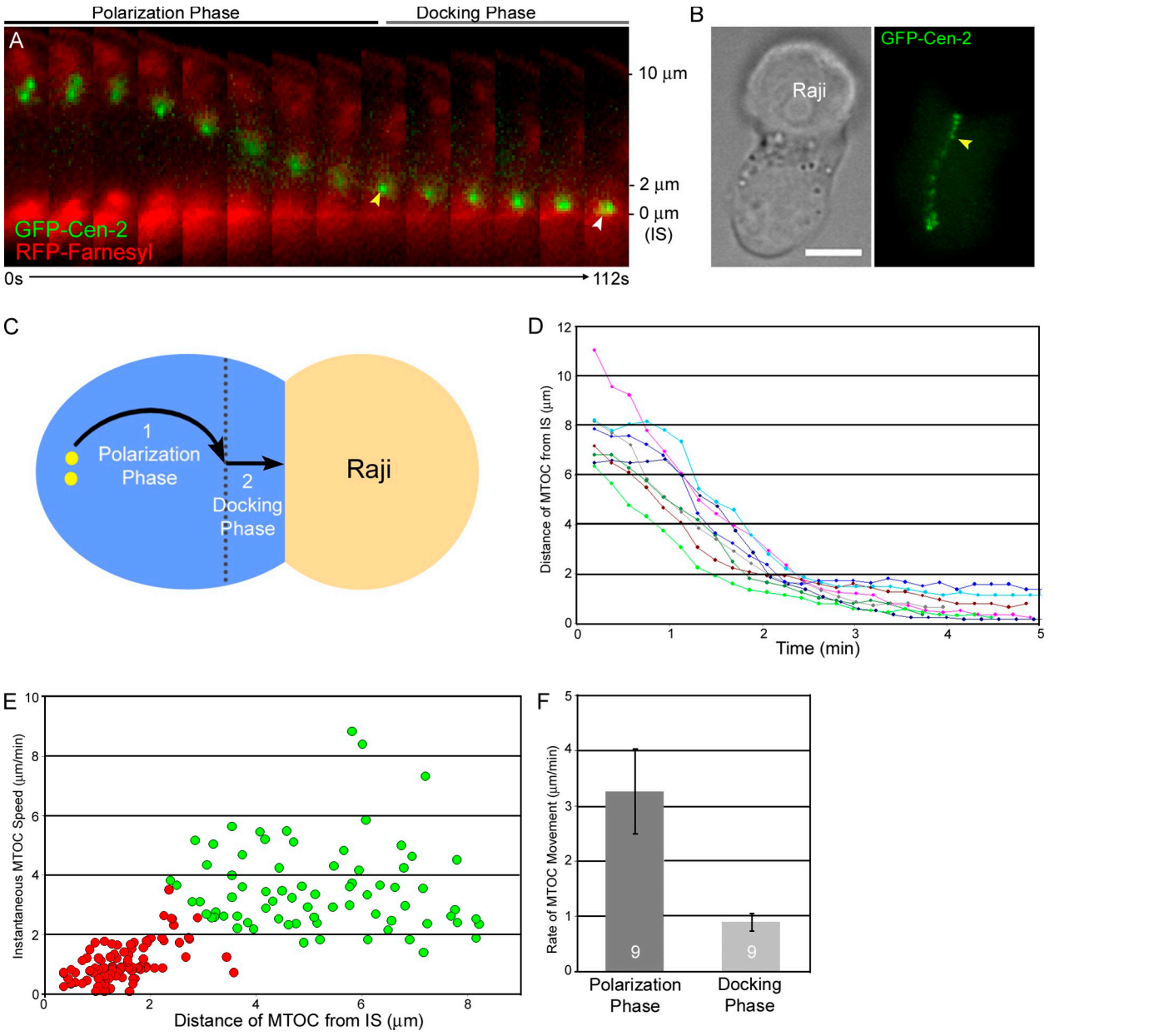

Figure 3. **MTOC repositioning is biphasic.** (A) Time-lapse montage showing MTOC repositioning in a representative Jurkat cell immediately after APC conjugation (merged image of the GFP-Cen-2–tagged MTOC and the RFP-Farnesyl–tagged synaptic membrane). The yellow and white arrowheads mark the transition between the polarization and docking phases and the docked MTOC, respectively. Distance from the IS is indicated on the right. See also Video 2. (B) Transmitted image of a Jurkat–Raji conjugate (left) and a maximum projection over time of the GFP-Cen-2 signal in the Jurkat (right). The yellow arrowhead marks the transition point between the two kinetic phases. (C) Cartoon depicting the two apparent kinetic phases. (D) Compilation of MTOC-repositioning events in eight additional conjugates, plotted as MTOC-to-IS distance versus time. (E) Scatter plot of the instantaneous speeds of MTOC movement as a function of MTOC-to-IS distance, obtained from the nine repositioning events presented in A and D. The red and green colors signify points grouped into the polarization and docking phases, respectively, as defined by statistical analyses (see text). (F) The average rates of MTOC movement during the polarization and docking phases. We note that the scatter plot in Fig. 3 E suggests that the MTOC slows down even more as it gets very close to the IS. Bar, 10 µm.

two clusters is validated by independent evidence for the existence of the transition point in Fig. 6, where we find that the MTOC reproducibly stalls ~2.4 µm from the IS when dynein function is attenuated. Based on this and additional statistical analyses (Fig. S1), we conclude that MTOC repositioning in Jurkat T cells is biphasic. Finally, the average MTOC-to-IS distance 10 min after APC conjugation was 0.68 ± 0.2 µm, consistent with Stinchcombe et al. (2006).

Imaging of "frustrated" APC–T cell conjugates suggests that a strong pulling force exists at the center of the IS

About 8% of control Raji–Jurkat conjugates were scored as no repositioning (Fig. 2 B). In every such case, the MTOC appears to be "stuck" behind the nucleus, possibly because the pulling forces on the MTOC from microtubules in contact with dynein at the IS are so symmetrical that an imbalance in pulling forces

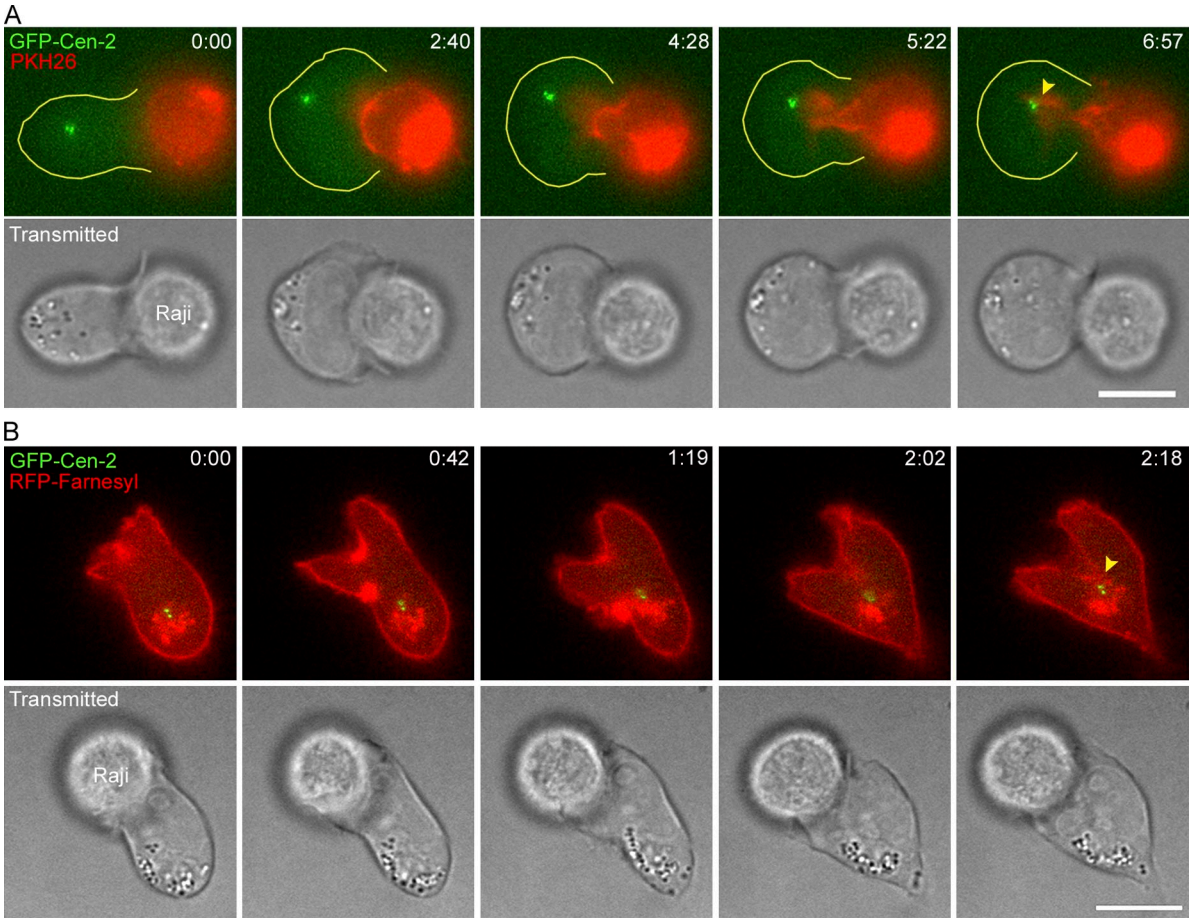

Figure 4. **Invagination of the IS membrane in frustrated conjugates.** Time-lapse montages showing the large invagination of the center of the IS interface in frustrated Jurkat–Raji conjugates where the Raji cell membrane has been labeled with the membrane dye PKH26 (A) or the Jurkat membrane has been labeled with RFP-Farnesyl (B). The yellow arrowheads mark the close approximation of the labeled membranes to the GFP-Cen-2–marked MTOC that has stalled on the back side of the nucleus. See also Videos 3 and 4. Bar, 10 µm.

required to commit to a certain path around the nucleus could not occur. To further investigate these "no repositioning" events, we marked the plasma membrane of the Raji cell with the red membrane dye PKH26. Strikingly, in three of four such "no repositioning" events, the Raji cell membrane was seen to dramatically invaginate into the Jurkat T cell (Fig. 4 A; Video 3), with the tip of the red invagination eventually reaching a point close to the T cell's green MTOC (Fig. 4 A, yellow arrowhead, frame 6:57). Similar deformations of the synaptic interface were observed in frustrated conjugates in which the T cell's plasma membrane had been labeled using farnesylated RFP (Fig. 4 B; see the yellow arrowhead marking the tip of the invagination at the center of the IS, frame 2:18; Video 4). As expected, therefore, the plasma membranes of both the APC and T cell invaginate into the T cell when MTOC repositioning is impeded.

These observations in frustrated Jurkat–Raji conjugates are important for several reasons. First, they argue that even "no repositioning" events can be considered as a form of MTOC repositioning, except that in this case it is the site of contact between the two cells that repositions. Second, they suggest that the force driving MTOC repositioning can be quite strong. Third, they are completely consistent with the idea that the site of force generation driving centrosome repositioning resides at the IS, as proposed previously (Kuhn and Poenie, 2002). Finally, and most importantly, they argue that this force generator is focused primarily near or at the center of the IS rather than at the periphery of the IS, as argued previously (Kuhn and Poenie, 2002; Combs et al., 2006).

The organization of microtubules in Jurkat–APC conjugates undergoing MTOC repositioning is consistent with a microtubule end-on capture-shrinkage mechanism driving repositioning

Previous studies using fixed and stained end-stage conjugates argue that dynein anchored at the periphery of the IS reels the centrosome in by pulling on the microtubule lattice, i.e., via a peripheral cortical sliding mechanism (Kuhn and Poenie, 2002). Given the results above, we decided to examine the dynamic organization of the microtubule cytoskeleton during MTOC repositioning in trap-engaged Jurkats expressing RFP-Pericentrin and 3×GFP-tagged EMTB to mark the T cell's centrosome and microtubules, respectively (Fig. 5 A). Control experiments (Figs. S2 and S3) indicated that, as reported previously (Faire et al., 1999), the expression of 3×GFP-EMTB does not alter

microtubule dynamics or organization. Immediately after conjugation, we observed several microtubules that project from the centrosome toward the APC (Fig. 5 A, inset, white arrows, 0 s frame) and that terminate in end-on fashion at the approximate center of the IS (Fig. 5 A, compare yellow arrowheads in the phase and fluorescent images). Over the next ∼30 s, these microtubules straightened and came together to form an apparent bundle of microtubules (referred to below as the microtubule "stalk") that terminates in end-on fashion near the center of the IS (follow the white arrows in the insets). Most importantly, microtubule stalks were then observed to undergo shortening (Fig. 5 B; follow the yellow arrowhead marking the point of contact of the stalk with the IS relative to the position of the yellow centrosome), causing the IS and centrosome to approach each other (in this case the IS interface came toward the centrosome). Fig. 5 C shows a clear example of an event where a shortening microtubule stalk pulled the centrosome all the way to the IS (the white arrow points to the centrosome, as inferred from the EMTB signal, whereas the yellow arrowhead points to the site where the green microtubule stalk terminates at the red IS, as inferred from the signal for farnesylated RFP; Video 5). We observed such perpendicular, centrally anchored, shortening microtubule stalks coincident with MTOC repositioning in 88.5% of conjugates (n = 26). Moreover, the rates at which these 3×GFP-EMTB–labeled microtubule stalks shortened matched the rates of MTOC repositioning presented in Fig. 3 F (3.22 ± 1.16 µm/min [n = 3] during the polarization phase and 1.22 ± 1.16 µm/min [n = 3] during the docking phase; $P > 0.05$ versus Fig. 3 F). Together, these results are consistent with MTOC repositioning being driven by a pulling force involving the end-on capture of microtubules at the approximate center of the IS, coupled with microtubule plus-end depolymerization, i.e., the capture-shrinkage mechanism, rather than with a cortical sliding mechanism involving microtubules approaching the IS at shallow angles near the edge of the IS.

Efforts to localize dynein at the spot where these microtubule stalks contact the IS were unsuccessful (although see Fig. S2 D), possibly because the number of dynein molecules there is very small. Recently, Howard and colleagues showed in *C. elegans* embryos that small membrane invaginations appear at the presumptive sites where the microtubule plus end is engaged at the cortex with the dynein-containing cortical force–generating unit (Redemann et al., 2010). These invaginations, which are presumably driven by the same force thought to pull the spindle toward the posterior of the embryo, i.e., the stepping of dynein while attached to a depolymerizing microtubule plus end, serve as an indirect readout of a focused cortical pulling force. Given their results, and our images of frustrated Jurkat–APC conjugates (Fig. 4), we asked if small invaginations at the IS can occur during normal repositioning events, and whether their position at the IS coincides with the end of the shortening microtubule stalk abutting the IS. To accomplish this, we imaged APC-conjugated Jurkats transfected with farnesylated RFP to mark the T cell's plasma membrane, as well as with 3×GFP-EMTB. One such example corresponds to the conjugate in Fig. 5 C discussed above, where the plasma membrane of the Jurkat cell does indeed exhibit a small invagination/indentation at the IS as the microtubule stalk undergoes shortening. Moreover, this membrane indentation coincides precisely with the site where the microtubule stalk abuts the IS. This can be seen best in the split image for the conjugate at 45 s (Fig. 5 D, see yellow arrows). Similar results were obtained when we marked the Raji cell plasma membrane with Far-Red Cellvue (see the "nipple-like" protrusion of the APC's plasma membrane exactly across from where the microtubule stalk in the Jurkat cell abuts the IS in Fig. 5 E). Together, these results provide visual support for the existence of a cortical pulling force being generated precisely at the site where the microtubule stalk contacts the IS membrane, further supporting a capture-shrinkage mechanism.

Inhibition of dynein impairs the polarization phase and blocks the docking phase of MTOC repositioning

The capture-shrinkage mechanism appears to require both dynein stepping and microtubule depolymerization to function in vivo (Nguyen-Ngoc et al., 2007) and in vitro (Laan et al., 2012). Therefore, if MTOC repositioning in T cells is driven by this mechanism, it should be blocked, or at least strongly impaired, by inhibiting either dynein or microtubule depolymerization. To address this, we first revisited the role of dynein in MTOC repositioning using the recently described, cell-permeant inhibitor of cytoplasmic dynein, Ciliobrevin-D, together with its inactive analogue CMP-2 as a control (Firestone et al., 2012). Control experiments showed that 30 min treatment of Jurkats with 50 µM Ciliobrevin-D does not perturb microtubule organization, including the focusing of microtubule minus ends at the centrosome (Fig. S2 A), or microtubule plus-end dynamics (Fig. S3 and Table S1). It does, however, inhibit the dynein-dependent centering of the Golgi apparatus and lysosomes (Fig. S2 B), as well as the normal accumulation of dynein at the centrosome (Fig. S2 C). Fig. 6 A shows that 50 µM Ciliobrevin-D results in a dramatic reduction in the frequency of full/APC repositioning events (5% of total events), as compared with untreated cells (87.6% of total events; see Fig. 2 B) and cells treated with the inactive analogue (90% of total events; Fig. 6 A). Scoring MTOC repositioning 30 min after conjugate formation (Fig. 6 B) rather than 10 min after (Fig. 6 A) yielded a more modest inhibition, suggesting that Ciliobrevin-D decreases the speed of MTOC repositioning. Consistently, Fig. 6 C shows that Ciliobrevin-D–treated cells exhibit a 65.5% reduction in the speed of MTOC movement during the polarization phase relative to control CMP-2–treated cells (Ciliobrevin-D, 1.10 ± 0.16 µm/min; CMP-2, 3.22 ± 0.82 µm/min; $P < 0.001$; calculated using only advances of one or more pixels per frame in the direction of the APC; see Materials and methods). Unlike untreated cells (Fig. 3 A) and CMP-2–treated cells (unpublished data), Ciliobrevin-D–treated cells exhibit pauses in MTOC movement and occasional movements of the MTOC away from the synapse (Fig. 6 E, white arrowheads). When such pauses/reversals are included in the calculation of MTOC speeds, Ciliobrevin-D–treated cells exhibit a 76.6% reduction in MTOC speed during the polarization phase (Ciliobrevin-D, 0.66 ± 0.49 µm/min; CMP-2, 2.83 ± 1.29 µm/min; $P < 0.001$).

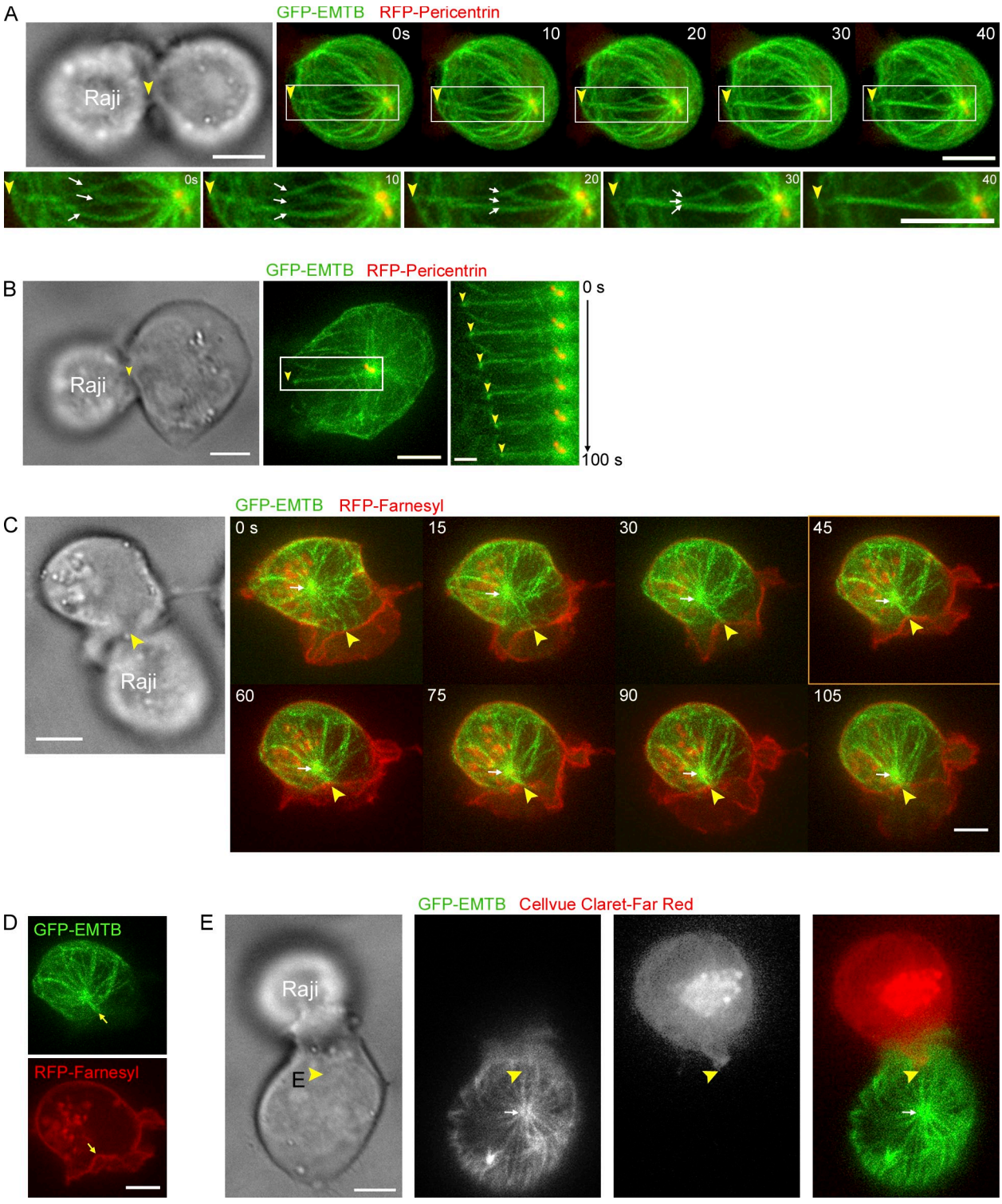

Figure 5. **Microtubule dynamics during MTOC repositioning.** (A) Time-lapse images of a Jurkat–Raji conjugate (transmitted image) in which the Jurkat has been labeled with 3×GFP-EMTB to mark microtubules and RFP-Pericentrin to mark the MTOC (which appears yellow) (fluorescent images). Zoomed images of the boxed regions in the fluorescent images are shown underneath. The white arrows point to the straightening microtubules, and the yellow arrowheads point to the center of the IS where these microtubules abut. (B) As in A, but including a kymograph demonstrating the shortening of the straight microtubule stalk. (C) As in A, except the Jurkat has been labeled with 3×GFP-EMTB to mark microtubules and RFP-Farnesyl to mark the plasma membrane. The position of the MTOC, as inferred from the 3×GFP-EMTB signal, is marked with a white arrow. Yellow arrowheads point to the center of the IS contacted by the straight, shortening microtubule stalk. See also Video 5. (D) A split version of the 45-s image in C showing the colocalization (see arrows) between the tip of the straight, shortening microtubule stalk (green) and an invagination of the Jurkat's plasma membrane (red) at the IS center. (E) As in A, except the Jurkat has been labeled with 3×GFP-EMTB and the Raji cell's plasma membrane has been labeled with the membrane dye Cellvue Claret-Far Red. The yellow arrowheads mark the "nipple-like" protrusion of the Raji cell's plasma membrane exactly across from where the microtubule stalk in the Jurkat cell abuts the IS. Bars: (A, C, and D) 5 µm; (B) 1 µm.

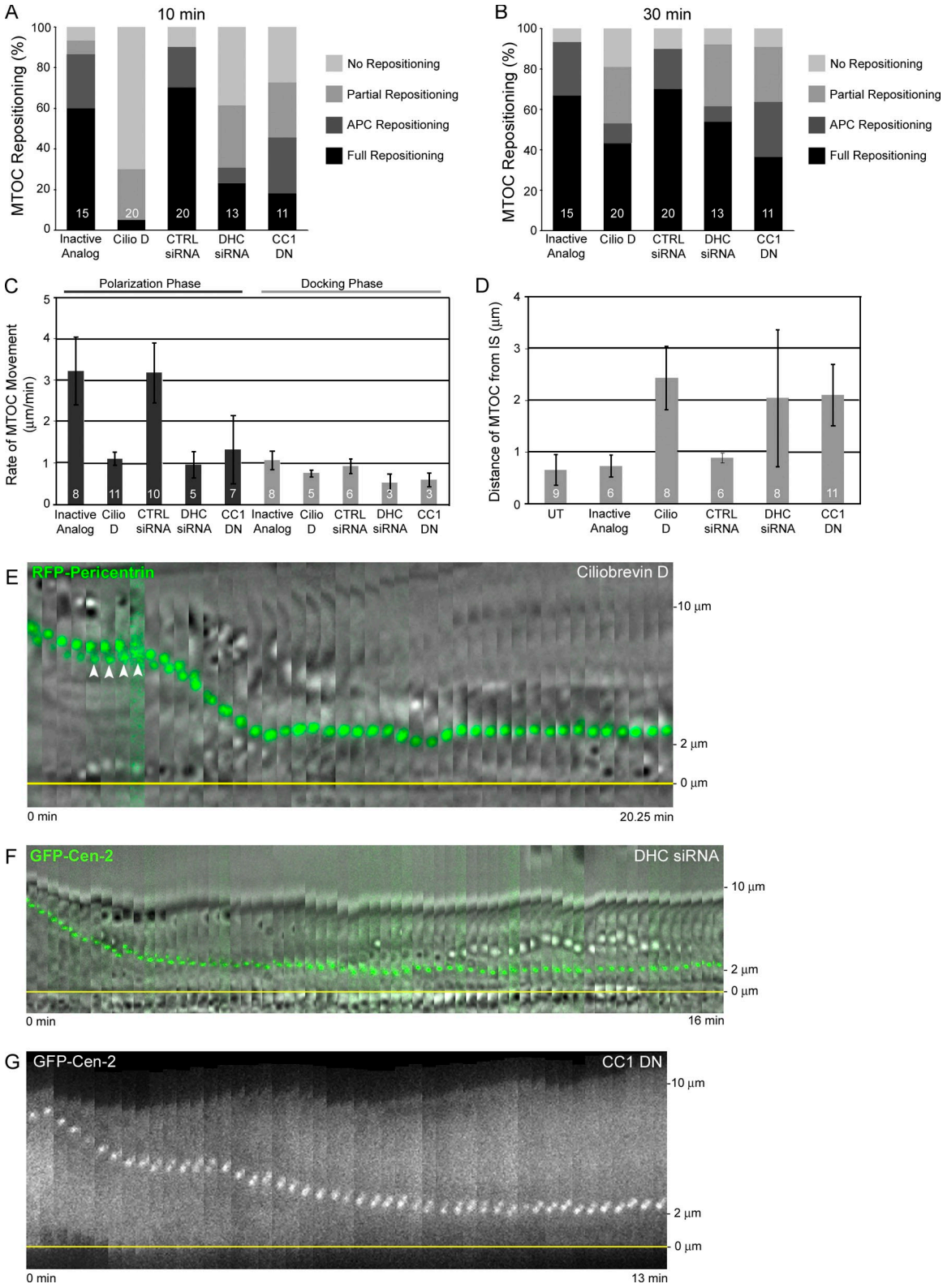

Figure 6. **Effect of dynein inhibition on MTOC repositioning.** (A) Shown are the percent contributions of the four classes of MTOC repositioning scored 10 min after conjugation with +SEE Raji cells for Jurkats treated with CMP-2 (Inactive Analogue), Ciliobrevin-D (Cilio D), control siRNA (CTRL siRNA), siRNA against the dynein heavy chain (DHC siRNA), or overexpressing a dominant-negative fragment of p150 glued (CC1 DN). (B) Same as in A, except scored 30 min after conjugation. (C) Rates of MTOC movement during the polarization and docking phases. (D) MTOC-to-IS distance 10 min (untreated [UT] and Inactive Analogue) and 30 min (Cilio D, CTRL siRNA, DHC siRNA, CC1-DN) after conjugation. (E) Time-lapse montage showing MTOC repositioning in a representative conjugate containing a Jurkat cell treated with Ciliobrevin-D (merge of the transmitted image and the RFP-Pericentrin–labeled MTOC pseudocolored green). (F) As in E, except the Jurkat has been transfected with DHC-siRNA and the MTOC was labeled with GFP-Cen-2. (G) As in F, except the Jurkat was overexpressing RFP-CC1-DN. The yellow lines in E–G mark the IS membrane. The white arrowheads in E point to pauses and reversals in MTOC movement. The values for DHC siRNA and CC1-DN versus Cilo-D, and for CTRL siRNA versus CMP-2, were not statistically different. All data were obtained from at least three independent experiments.

Time-lapse montages like the one in Fig. 6 E also reveal the second major defect in Ciliobrevin-D–treated cells: a general failure to undergo the docking phase of MTOC repositioning. Specifically, while WT cells like the one shown in Fig. 3 A typically exhibit a docked centrosome, the centrosome in the Ciliobrevin-D–treated cell shown in Fig. 6 E has stalled ∼2 µm away from the IS membrane, i.e., at the boundary between the polarization and docking phases of MTOC repositioning. This observation was supported by quantitation (Fig. 6 D), as untreated and CMP-2–treated cells exhibit average MTOC-to-IS distances 10 min after conjugate formation of 0.66 ± 0.30 µm and 0.73 ± 0.20 µm, respectively, while Ciliobrevin-D–treated cells exhibit an average MTOC-to-IS distance 30 min after conjugate formation of 2.43 ± 0.60 µm ($P < 0.001$ versus both controls). Importantly, this latter distance coincides with the normal transition point between the polarization and docking phases (Fig. 3), arguing that dynein-inhibited cells are defective in docking. That said, Ciliobrevin-D–treated cells occasionally make transient forays past the transition point. Quantification of the speed of these rare, transient docking movements showed that they are significantly slower (Fig. 6 C, docking phase).

To confirm the Ciliobrevin-D data, we used two additional approaches to inhibit dynein function: (1) siRNA-mediated knockdown of the dynein heavy chain, together with an siRNA control (see also Fig. S2 E), and (2) the overexpression of RFP-tagged CC1, a fragment of the dynactin subunit p150/glued, which may inhibit dynein function in dominant-negative fashion by shielding dynein from its two key regulatory factors, dynactin and LIS1/Ndel (Vallee et al., 2012). Importantly, Fig. 6, A–G, show that in every qualitative and quantitative measure, including an essentially complete abrogation of the docking phase, these two forms of dynein inhibition phenocopied the results obtained with Ciliobrevin-D (see figure legend for details). Together, these inhibition experiments indicate that dynein plays a major role in driving MTOC repositioning and docking in Jurkat T cells.

Inhibition of MT depolymerization using taxol impairs MTOC movement during both the polarization and docking phases of MTOC repositioning

To provide further support for the capture-shrinkage mechanism, we tested the effect of taxol, a known inhibitor of microtubule depolymerization, on MTOC repositioning. Control experiments (Fig. S4) indicated that a 15-min preincubation with 0.5 µM taxol (Fig. S4 B and Video 6) represented the best compromise between taxol's tendency at high concentrations to bundle microtubules (Fig. S4 A) and the addition of too little taxol to effectively block depolymerization. Importantly, 0.5 µM taxol did not alter microtubule organization, including the focusing of microtubule minus ends at the centrosome (Fig. S4 C), or the rate of microtubule plus-end growth (Fig. S3 A). As expected, however, it dramatically reduced the frequency of microtubule catastrophes initiated at the microtubule plus end (Table S1 A). Fig. 7 A shows that whereas DMSO-treated cells exhibited robust MTOC movement after APC engagement (100% full/APC repositioning), taxol-treated cells exhibited only 39 and 50% full/APC repositioning after 10 and 30 min of APC engagement, respectively. Moreover, taxol-treated cells exhibited a 71% reduction in the speed of MTOC movement during the polarization phase relative to control DMSO-treated cells (DMSO, 3.55 ± 0.1.27 µm/min; taxol, 1.03 ± 0.33 µm/min; see polarization phase in Fig. 7 B; $P < 0.001$). Of note, the magnitude of these inhibitions is quite similar to those observed in dynein-inhibited cells. That said, although dynein inhibition blocked the progression of MTOC movement through the docking phase, taxol treatment did not, as evidenced by time-lapse montages of DMSO- and taxol-treated cells such as the ones in Fig. 7, D and E, respectively (docking indicated by yellow arrowhead). Consistently, the MTOC-to-IS distance 10 min after APC engagement was statistically the same between taxol-treated and DMSO-treated cells (DMSO, 0.8 ± 0.24 µm; taxol, 0.89 ± 0.39 µm; see Fig. 7 C; $P > 0.05$; also, neither is statistically different from untreated cells). Taxol-treated cells did, however, exhibit an ∼62.2% reduction in the speed of MTOC movement during the docking phase relative to control DMSO-treated cells (DMSO, 1.14 ± 0.22 µm/min; taxol, 0.43 ± 0.09 µm/min; see docking phase in Fig. 7 B; $P < 0.001$). Together, these results show that microtubule depolymerization also plays an important role in driving MTOC repositioning in Jurkat T cells, consistent with the capture-shrinkage mechanism.

Dual inhibition of dynein and microtubule depolymerization leads to a profound block in MTOC repositioning

We next tested the effect on MTOC repositioning of inhibiting both dynein and microtubule depolymerization simultaneously using a combination of Ciliobrevin-D and taxol. Fig. 7 A shows that combined treatment with 50 µM Ciliobrevin-D and 0.5 µM taxol results in a total inhibition of full/APC repositioning at both 10 and 30 min after APC conjugation ($P < 0.001$). This complete inhibition of MTOC repositioning is evident in typical time-lapse montages such as the one in Fig. 7 F. Although a rate for MTOC repositioning in full repositioning events could obviously not be obtained, the rate of MTOC movement during the small number of partial repositioning events observed in these cells (0.45 ± 0.18 µm/min) was approximately sevenfold slower than in untreated and DMSO-treated cells, and approximately threefold slower than in cells treated with either Ciliobrevin-D or taxol alone. Together, these results show that both dynein function and microtubule depolymerization are required for efficient MTOC repositioning in Jurkat T cells, consistent with the capture-shrinkage mechanism.

Inhibition of microtubule polymerization impairs MTOC repositioning

Finally, the initiation, and possibly progression, of microtubule end-on capture-shrinkage could depend significantly on dynamic microtubule plus ends, which are thought to drive microtubule search-capture at the cell cortex (Wu et al., 2006). To test this possibility, we scored MTOC repositioning in the presence of a low dose of nocodazole (100 nM). As expected, this dose blocked growth at microtubule plus ends (Table S1 B) without depolymerizing the microtubule network (Fig. S4 D) or

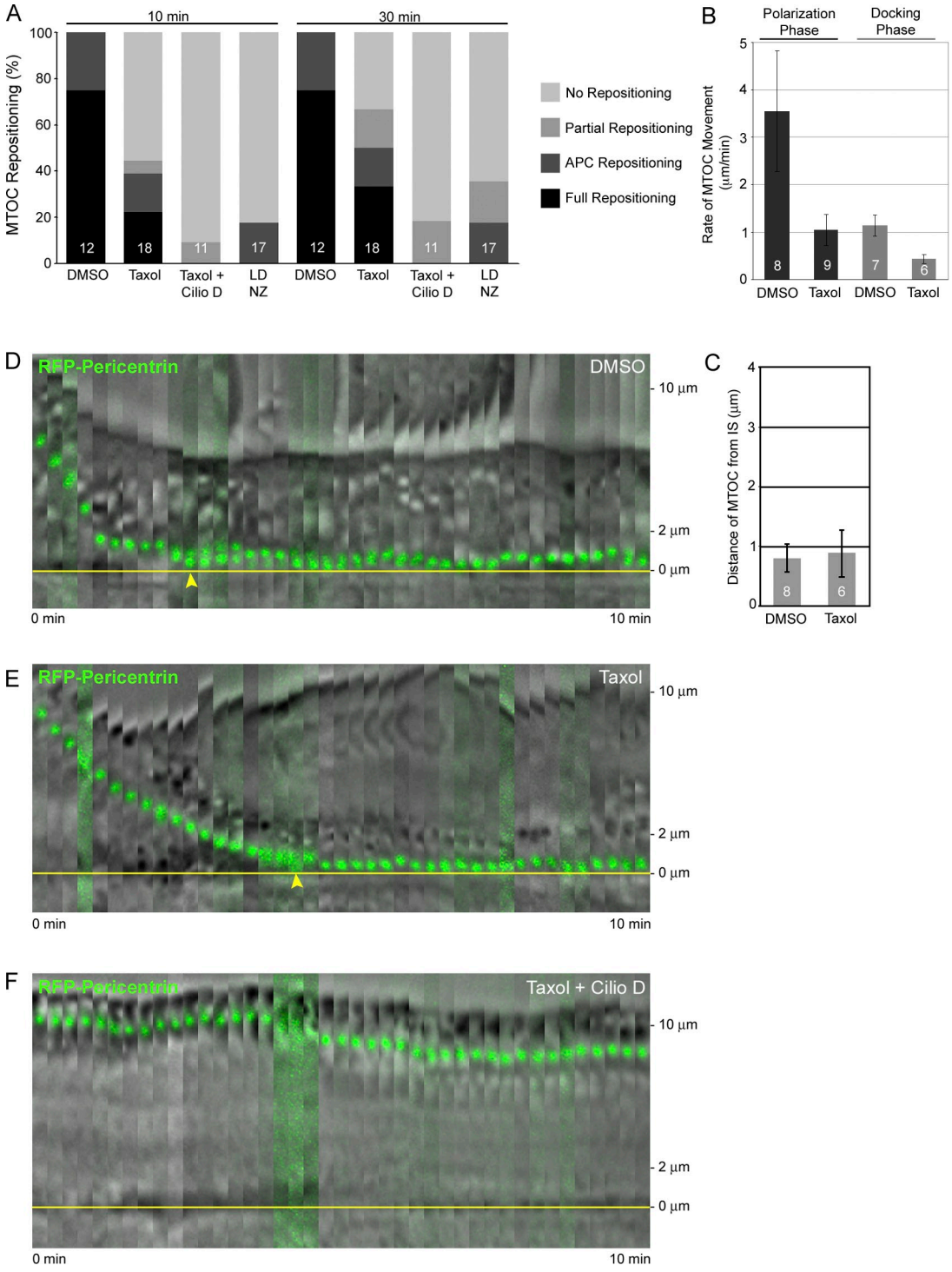

Figure 7. **Effects of taxol, combined taxol/Ciliobrevin-D, and low dose nocodazole on MTOC repositioning.** (A) Shown are the percent contributions of the four classes of MTOC repositioning scored 10 min (left) and 30 min (right) after conjugation with +SEE Raji cells for Jurkats treated with DMSO, taxol, taxol plus Ciliobrevin-D (Taxol + Cilio D), or low dose nocodazole (LD NZ). (B) Rates of MTOC movement during the polarization and docking phases. (C) MTOC-to-IS distance 30 min after conjugation. (D) Time-lapse montage showing MTOC repositioning in a representative conjugate containing a Jurkat cell treated with DMSO (each frame is a merge of the transmitted image and the RFP-Pericentrin–labeled MTOC pseudocolored green). (E) As in D, except the Jurkat has been treated with taxol. (F) As in D, except the Jurkat has been treated with taxol and Ciliobrevin-D. The yellow lines in D–F mark the IS membrane. All data were obtained from at least three independent experiments.

changing either the frequency (Table S1 A) or rate (Fig. S3 B) of microtubule depolymerization. Importantly, low dose nocodazole treatment resulted in a dramatic reduction in the frequency of full/APC repositioning events 10 min (18% of total events) and 30 min (19% of total events) after conjugate formation relative to the DMSO control (100% of total events at both time points; see "LD NZ" in Fig. 7 A). These observations argue that the search and capture of microtubule plus ends at the cortex, which is driven by dynamic microtubule plus ends, is important for MTOC repositioning in Jurkat T cells.

Discussion

Here we sought to define the mechanism of dynein-dependent MTOC repositioning in Jurkat T cells using optical tweezers to provide both temporal and spatial control over APC presentation. Importantly, our results challenge a number of previous conclusions regarding MTOC repositioning in T cells. First, robust MTOC repositioning requires signaling downstream from both the TCR and LFA-1 (see also Tsun et al., 2011), not just the TCR (Combs et al., 2006). Our results also indicate that the normal rise in intracellular calcium concentration after TCR engagement is required for robust MTOC repositioning, in contrast to a recent report (Quann et al., 2009).

Second, MTOC repositioning involves two distinct kinetic phases, not one as reported previously (3.6 ± 1.1 µm/min, Kuhn and Poenie, 2002; ∼3 µm/min, Quann et al., 2009). Specifically, repositioning involves a fast (∼3.3 µm/min) polarization phase and a slower (∼0.9 µm/min) docking phase, with a transition between them occurring at ∼2.2 µm from the IS. Independent support for the existence of this transition point was provided by the observation that the MTOC reproducibly stalls ∼2.4 µm from the IS when dynein function is attenuated. Interestingly, Griffiths and colleagues have shown that signaling through Lck controls the progression of the partially repositioned MTOC through a docking step required for its close approach to the IS (Tsun et al., 2011).

Third, and most importantly, we present evidence that MTOC repositioning in T cells is driven by a microtubule end-on capture-shrinkage mechanism focused at the center of the IS rather than a cortical sliding mechanism focused at the periphery of the IS, as reported previously (Kuhn and Poenie, 2002; Combs et al., 2006). Four lines of evidence support this conclusion. First, the striking invagination of the center of the IS membrane in the direction of the centrosome observed in "frustrated" Jurkat–APC conjugates argues strongly that the force-generating mechanism driving MTOC repositioning is focused at the center of the IS and not its periphery. Second, dynamic imaging of microtubules during normal MTOC repositioning revealed microtubule end-on attachments near or at the center of the IS that are followed by the shortening of these microtubules, thereby drawing the centrosome to the IS. These dynamic images are consistent with MTOC repositioning being driven by the capture-shrinkage mechanism focused at the center of the IS and not with the cortical sliding mechanism operating at the IS periphery. Third, we observed small invaginations of the IS membrane at the point where the shortening microtubules abut the IS, suggesting the presence of force generation there. Of note, these small invaginations may be related to the frequent, ∼1-µm deep T cell invaginations (and corresponding protrusions in the APC) seen at the center of the IS in T cell–APC conjugates during the first several minutes after productive contact (Singleton et al., 2006). Finally, inhibition of either dynein or microtubule depolymerization inhibited MTOC repositioning, consistent with the capture-shrinkage mechanism. Although these results argue strongly that the microtubule end-on capture-shrinkage mechanism plays a major role in MTOC repositioning in T cells, we cannot rigorously exclude the possibility that the cortical sliding of microtubules (Kuhn and Poenie, 2002) makes some contribution to the process.

As currently envisioned, the capture-shrinkage mechanism obligatorily couples the stepping of cortically anchored dynein attached to the microtubule plus end with the depolymerization of this end to create the pulling force on the centrosome (Laan et al., 2012). This mechanism should, therefore, be fully abrogated by complete inhibition of either dynein or microtubule depolymerization. We attribute the partial inhibitions of MTOC repositioning we saw with Ciliobrevin-D or taxol treatment as being due to partial inhibitions of dynein and (especially) microtubule depolymerization, respectively. This interpretation is consistent with the partial effects on asymmetric spindle positioning seen in *C. elegans* embryos treated with taxol or after dynein inactivation (Nguyen-Ngoc et al., 2007). Alternatively, our inhibition studies could be interpreted as evidence of two parallel, partially redundant pathways driving MTOC repositioning in Jurkats—one driven by dynein and one by microtubule depolymerization—although we do not favor this idea. The partial inhibitions could also reflect the contribution of a microtubule-independent pathway to MTOC repositioning (e.g., some form of actomyosin-dependent contribution), although the total cessation of centrosome repositioning we observed with combined Ciliobrevin-D/taxol treatment does not seem to support that idea. Finally, given that MTOC repositioning itself helps drive sustained T cell signaling (Martín-Cófreces et al., 2008), we cannot exclude some contribution of reduced signaling to the defects seen in Ciliobrevin-D– and taxol-treated cells.

For several teleological reasons we think that the microtubule end-on capture-shrinkage mechanism makes more sense than the cortical sliding mechanism for driving MTOC repositioning. First, because the force vector in end-on capture-shrinkage is perpendicular to the plane of the membrane, the path of least resistance should usually be centrosome repositioning. By contrast, in the cortical sliding mechanism, where the force vector should often be nearly parallel to the plane of the membrane, the path of least resistance will often be the sliding of dynein's anchor point in the plane of the membrane rather than MTOC repositioning. Second, it is hard to imagine how a cortical sliding mechanism could avoid microtubules being pulled in a variety of different directions across the IS interface, significantly reducing the efficiency and reproducibility of the process. Finally, for this same reason, the capture-shrinkage mechanism seems more consistent with the relatively constant and highly reproducible speed of MTOC movement seen during the polarization phase.

We think the biphasic nature of MTOC repositioning reflects a force–velocity relationship in which the emergence of a resistive force around 2 µm from the IS causes the centrosome to move at a slower speed during the docking phase. The emergence of this resistive force is sometimes abrupt, leading to a sharp reduction in speed, and other times not, leading to a more gradual reduction in speed. This resistive force also results in a differential sensitivity to partial dynein inhibition, with the "high" force docking phase being more sensitive (i.e., completely inhibited) than the "low" force polarization phase (partially inhibited). Candidate resistive forces

include physical impediments to MTOC progression (e.g., organelles in the way) or the emergence of a force that opposes dynein at the IS (e.g., dynein on the nuclear envelope; although see Lui-Roberts et al., 2012, who showed that MTOC–nuclear envelope interaction in T cells is minimal).

Several aspects of our work merit further investigation. These include identifying the nature of dynein's cortical anchor (Combs et al., 2006; Nguyen-Ngoc et al., 2007), looking for the possible contribution of a depolymerizing kinesin (Ten Hoopen et al., 2012), and addressing the possible role of Lis1, which appears to be required for dynein to exhibit high force (Vallee et al., 2012), and which is part of the capture-shrinkage mechanism in the *C. elegans* embryo (Nguyen-Ngoc et al., 2007).

In summary, we present evidence that MTOC repositioning in Jurkat T cells is driven predominantly by the microtubule end-on capture-shrinkage mechanism, where the stepping of cortically anchored dynein attached to the plus end of the microtubule, coupled with microtubule plus-end depolymerization, creates in a mutual and interdependent fashion the pulling force on the centrosome (Laan et al., 2012). The mechanism is focused at the center of the IS and not at its periphery, and drives a repositioning process possessing two kinetic phases that rapidly and robustly draws the centrosome to the IS membrane to support the vectorial delivery of effector molecules.

Materials and methods

Cell culture, transfection, plasmids, and reagents

E6.1, JCAM2.5, and JB2.7 Jurkat T cells and Raji B cells (gifts from Larry Samelson [NIH, Bethesda, MD] and Martin Poenie [University of Texas, Austin, TX]) were cultured at 37°C in IMDM media (#12440; Invitrogen) supplemented with fetal bovine serum (#F0392; Sigma-Aldrich), sodium pyruvate (#11360; Invitrogen), L-glutamine (#25030; Invitrogen), penicillin/streptomycin (#15140; Invitrogen), and MEM nonessential amino acids solution (#11140; Invitrogen). Jurkat T cells and Raji B cells were replated every 48 h at a concentration of 2.0×10^5 cells/ml and 4.0×10^5 cells/ml, respectively. Transfections were performed by nucleofection using cells at a concentration of 1.0×10^6 cells/ml, 1–3 µg of plasmid DNA, Amaxa Kit V (Lonza), and the electroporation protocol for Jurkat T cells (Yi et al., 2012). Centrin-2 in mEGFP-C1 or mRFP-C1, farnesylated mRFP-C1, CC1-mRFP-C1, LFA-1α-EGFP-N1, EMTB-3xEGFP-C1, pericentrin–mRFP-C1, dynein intermediate chain 2C-mEGFP-N1 (DIC-2C-GFP), EB3-mCherry-N1, and TGN38-mCherry-N1 were gifts of Jose Martina (NIH), Julie Donaldson (NIH), Trina Schroer (Johns Hopkins University, Baltimore, MD), Minsoo Kim (University of Rochester, Rochester, NY), Chloe Bulinski (Columbia University, New York, NY), Clare Waterman (NIH), Kevin Pfister (University of Virginia, Charlottesville, VA), Yuko Mimori-Kiyosue (KAN Research Institute, Kobe, Japan), and Jennifer Lippincott-Schwartz (NIH), respectively. Taxol (P3456), Fluo-4 AM (F14217), BAPTA-AM (B-1205), and LysoTracker red (L-7528) were purchased from Invitrogen. Staphylococcal enterotoxin E (SEE; ET 404) was purchased from Toxin Technology, and the dyes PKH26 (MINI26-1KT) and CellVue Clarat (MINCLARET-1KT), as well as fibronectin (F2006), were purchased from Sigma-Aldrich. The On-Target Plus Smart Pool siRNA directed against human dynein heavy chain (L-006828-00-005) was purchased from Thermo Fisher Scientific, and the negative control siRNA (AM4611) was purchased from Ambion. The monoclonal antibody to the dynein heavy chain was purchased from Sigma-Aldrich (D1667). For Western blotting, whole-cell extracts were resolved on 6% Tris-glycine polyacrylamide gels (EC6068; Invitrogen), transferred to nitrocellulose using a semi-dry blotter (model SD; Bio-Rad Laboratories), incubated with the dynein heavy chain antibody, and developed using enhanced chemiluminescence (RPN2108; GE Healthcare), as described previously (Yi et. al., 2012).

Optical trap design

The optical trap was based on an early design from the laboratory of Steven Block (Spector et al., 1998). In brief, a Nd:YVO4 laser (4 W continuous power at 1064 nm) provides the IR beam, a Uniblitz shutter gates the laser to a 10× beam expander, a 1/2 λ waveplate coupled with a polarized beam splitter attenuates the laser power, and a 2× Keplerian beam expander allows complete filling of the back focal plane of the objective. In addition, two mirrors enable manual steering of the beam. Lastly, the objective lens (see below) focuses the beam onto the specimen stage, forming the gradient required for optical trapping. The beam effectively traps 3-µm-diameter polystyrene latex beads and Raji B cells at 1 mW and 25 mW of laser power, respectively.

Optical trap–controlled conjugate formation

Raji B cells were coated with SEE by incubation in cell culture media containing 2 µg/ml SEE for 1.5 h at 37°C, as described previously (Combs et al., 2006). To create the flow chamber, two strips of double-stick tape were placed on parallel edges of a glass slide and a no. 1.5 glass coverslip coated with fibronectin was placed on top. Jurkat cells were then introduced into the flow chamber and allowed to adhere to the coverslip for 2 min at 37°C. To create the conjugate, Raji cells were introduced into the flow chamber and a nearby floating Raji cell was trapped and steered such that its initial point of contact with the T cell was directly opposite from the position the T cell's fluorescent centrosome. The optical trap was then turned off and imaging commenced immediately (time zero).

Image acquisition

Images were acquired at 10–30 frame/s in cell culture media supplemented with 40 µM Hepes using either a 60× (1.40 NA), 100× (1.42 NA), or 150× (1.45 NA) objective on a microscope (IX8; Olympus) fitted with a spinning disk confocal head (CSU-X1; Yokogawa Corporation of America) and a camera (QuantEM 512SC; Photometrix) and controlled by MetaMorph software. Stage temperature was maintained at 37°C using a Nevtek stage heater. For imaging MTOC repositioning, the focal plane was occasionally adjusted to maintain focus on the centrosome. For imaging the dynamics of the microtubule cytoskeleton, 3D time-lapse images (ten 1 µm-thick optical sections acquired over 3 s every 10 or 15 s) were obtained using a stage controller (NanoScan Z; Prior Scientific). For imaging intracellular calcium flux, Jurkat cells were loaded before conjugate formation with 5 µM Fluo-4AM for 60 min in cell culture medium and washed, as described by the manufacturer. Measurement of MTOC repositioning in the presence of EGTA and BAPTA-AM to chelate extracellular and intracellular calcium, respectively, was performed as described previously (Quann et al., 2009), except that 2 mM EGTA was used, Jurkats were preincubated in 50 µM BAPTA-AM for 20 min, and Fluo-4AM was also loaded to confirm the lack of intracellular calcium flux. We avoided the use of GFP-chimeras when imaging in the presence of Ciliobrevin-D, as blue light leads to cell toxicity (green light with RFP-chimeras is fine). Images were analyzed using MetaMorph software.

Analysis of MTOC movement

MTOC-to-IS distances were obtained by measuring the distance from the center of the fluorescent MTOC to the plane of contact between the Jurkat and Raji cell, obtained either from the bright-field image or from the position of the mRFP-Farnesyl–labeled T cell membrane. To obtain the instantaneous speed of MTOC movement, the MTOC-to-IS distance in each frame was subtracted from that in the previous frame and the product divided by the elapsed time between the two frames. Unless indicated otherwise, only positive pixel displacements (one or more pixels) in the direction of the IS were included in calculating speeds. Hierarchical cluster analysis was performed with Origin software, using Ward's Method and Squared Euclidean Distance Interval settings. The Calinski and Harabatz Index analysis was performed using the "fpc" package in R software, a Calinski and Harabatz Index of 2–6 cluster fits, and 20 rolling simulations. To obtain the point of transition between the two kinetic phases, the MTOC-to-IS distance at which the largest deceleration in the instantaneous velocity occurred was recorded and averaged in nine WT cells. Statistical significance was determined using the Student's *t* test.

Online supplemental material

Fig. S1 presents cluster analyses of the instantaneous MTOC speed data in Fig. 3 E, which argue that MTOC repositioning is biphasic. Fig. S2 shows that Ciliobrevin-D treatment does not alter microtubule organization but does inhibit basic dynein functions and the accumulation of dynein at the centrosome. Fig. S3 presents the dynamics of the microtubule plus end in the presence of Ciliobrevin-D, taxol, or low dose nocodazole. Fig. S4 shows that 0.5 µM taxol does not cause obvious microtubule bundling or defects in microtubule organization. Video 1 shows the repositioning of a Jurkat T cell's centrosome toward the IS after contact with an APC

that had been steered to the Jurkat using the optical trap. Video 2 shows the repositioning of a Jurkat T cell's centrosome toward the fluorescently tagged IS membrane after contact with an APC that had been steered to the Jurkat using the optical trap. Video 3 shows the protrusion of the APC's plasma membrane toward a stalled Jurkat T cell centrosome. Video 4 shows the invagination of the Jurkat T cell's plasma membrane toward its stalled centrosome. Video 5 shows the dynamics of microtubules as the MTOC repositions toward the IS in a Jurkat T cell after contact with an APC that had been steered to the Jurkat using the optical trap. Video 6 shows the dynamics of microtubules in a Jurkat T cell treated with 0.5 µM taxol and stimulated on an anti-CD3 antibody-coated coverslip surface. Table S1 shows the inhibition of catastrophe events at the microtubule plus end by taxol and the inhibition of dynamicity of microtubule plus ends by low dose nocodazole. Online supplemental material is available at http://www.jcb.org/cgi/content/full/jcb.201301004/DC1.

We thank all those who provided reagents; Rajat Varma, Lois Greene, and Evan Eisenberg for advice; Ikuko Fujiwara for cluster analyses; and Yasuharu Takagi and Kier Neuman for help with building the optical trap.

J.K. Chen gratefully acknowledges support from the National Institutes of Health/National Cancer Institute (R01 CA136574). T.M. Kapoor gratefully acknowledges support from the National Institutes of Health/National Institute of General Medical Sciences (RO1 GM65933).

Submitted: 2 January 2013
Accepted: 29 July 2013

References

Angus, K.L., and G.M. Griffiths. 2013. Cell polarisation and the immunological synapse. *Curr. Opin. Cell Biol.* 25:85–91. http://dx.doi.org/10.1016/j.ceb.2012.08.013

Blanchard, N., V. Di Bartolo, and C. Hivroz. 2002. In the immune synapse, ZAP-70 controls T cell polarization and recruitment of signaling proteins but not formation of the synaptic pattern. *Immunity*. 17:389–399. http://dx.doi.org/10.1016/S1074-7613(02)00421-1

Choudhuri, K., and M.L. Dustin. 2010. Signaling microdomains in T cells. *FEBS Lett.* 584:4823–4831. http://dx.doi.org/10.1016/j.febslet.2010.10.015

Combs, J., S.J. Kim, S. Tan, L.A. Ligon, E.L. Holzbaur, J. Kuhn, and M. Poenie. 2006. Recruitment of dynein to the Jurkat immunological synapse. *Proc. Natl. Acad. Sci. USA*. 103:14883–14888. http://dx.doi.org/10.1073/pnas.0600914103

Faire, K., C.M. Waterman-Storer, D. Gruber, D. Masson, E.D. Salmon, and J.C. Bulinski. 1999. E-MAP-115 (ensconsin) associates dynamically with microtubules in vivo and is not a physiological modulator of microtubule dynamics. *J. Cell Sci.* 112:4243–4255.

Firestone, A.J., J.S. Weinger, M. Maldonado, K. Barlan, L.D. Langston, M. O'Donnell, V.I. Gelfand, T.M. Kapoor, and J.K. Chen. 2012. Small-molecule inhibitors of the AAA+ ATPase motor cytoplasmic dynein. *Nature*. 484:125–129. http://dx.doi.org/10.1038/nature10936

Geiger, B., D. Rosen, and G. Berke. 1982. Spatial relationships of microtubule-organizing centers and the contact area of cytotoxic T lymphocytes and target cells. *J. Cell Biol.* 95:137–143. http://dx.doi.org/10.1083/jcb.95.1.137

Gönczy, P. 2008. Mechanisms of asymmetric cell division: flies and worms pave the way. *Nat. Rev. Mol. Cell Biol.* 9:355–366. http://dx.doi.org/10.1038/nrm2388

Grill, S.W., and A.A. Hyman. 2005. Spindle positioning by cortical pulling forces. *Dev. Cell*. 8:461–465. http://dx.doi.org/10.1016/j.devcel.2005.03.014

Hashimoto-Tane, A., T. Yokosuka, K. Sakata-Sogawa, M. Sakuma, C. Ishihara, M. Tokunaga, and T. Saito. 2011. Dynein-driven transport of T cell receptor microclusters regulates immune synapse formation and T cell activation. *Immunity*. 34:919–931. http://dx.doi.org/10.1016/j.immuni.2011.05.012

Huse, M. 2012. Microtubule-organizing center polarity and the immunological synapse: protein kinase C and beyond. *Front Immunol*. 3:235. http://dx.doi.org/10.3389/fimmu.2012.00235

Kuhn, J.R., and M. Poenie. 2002. Dynamic polarization of the microtubule cytoskeleton during CTL-mediated killing. *Immunity*. 16:111–121. http://dx.doi.org/10.1016/S1074-7613(02)00262-5

Kuhné, M.R., J. Lin, D. Yablonski, M.N. Mollenauer, L.I. Ehrlich, J. Huppa, M.M. Davis, and A. Weiss. 2003. Linker for activation of T cells, zeta-associated protein-70, and Src homology 2 domain-containing leukocyte protein-76 are required for TCR-induced microtubule-organizing center polarization. *J. Immunol.* 171:860–866.

Kupfer, A., G. Dennert, and S.J. Singer. 1983. Polarization of the Golgi apparatus and the microtubule-organizing center within cloned natural killer cells bound to their targets. *Proc. Natl. Acad. Sci. USA*. 80:7224–7228. http://dx.doi.org/10.1073/pnas.80.23.7224

Laan, L., N. Pavin, J. Husson, G. Romet-Lemonne, M. van Duijn, M.P. López, R.D. Vale, F. Jülicher, S.L. Reck-Peterson, and M. Dogterom. 2012. Cortical dynein controls microtubule dynamics to generate pulling forces that position microtubule asters. *Cell*. 148:502–514. http://dx.doi.org/10.1016/j.cell.2012.01.007

Li, R., and G.G. Gundersen. 2008. Beyond polymer polarity: how the cytoskeleton builds a polarized cell. *Nat. Rev. Mol. Cell Biol.* 9:860–873. http://dx.doi.org/10.1038/nrm2522

Lowin-Kropf, B., V.S. Shapiro, and A. Weiss. 1998. Cytoskeletal polarization of T cells is regulated by an immunoreceptor tyrosine-based activation motif-dependent mechanism. *J. Cell Biol.* 140:861–871. http://dx.doi.org/10.1083/jcb.140.4.861

Lui-Roberts, W.W., J.C. Stinchcombe, A.T. Ritter, A. Akhmanova, I. Karakesisoglou, and G.M. Griffiths. 2012. Cytotoxic T lymphocyte effector function is independent of nucleus-centrosome dissociation. *Eur. J. Immunol.* 42:2132–2141. http://dx.doi.org/10.1002/eji.201242525

Martín-Cófreces, N.B., D. Sancho, E. Fernández, M. Vicente-Manzanares, M. Gordón-Alonso, M.C. Montoya, F. Michel, O. Acuto, B. Alarcón, and F. Sánchez-Madrid. 2006. Role of Fyn in the rearrangement of tubulin cytoskeleton induced through TCR. *J. Immunol.* 176:4201–4207.

Martín-Cófreces, N.B., J. Robles-Valero, J.R. Cabrero, M. Mittelbrunn, M. Gordón-Alonso, C.H. Sung, B. Alarcón, J. Vázquez, and F. Sánchez-Madrid. 2008. MTOC translocation modulates IS formation and controls sustained T cell signaling. *J. Cell Biol.* 182:951–962. http://dx.doi.org/10.1083/jcb.200801014

Moore, J.K., and J.A. Cooper. 2010. Coordinating mitosis with cell polarity: Molecular motors at the cell cortex. *Semin. Cell Dev. Biol.* 21:283–289. http://dx.doi.org/10.1016/j.semcdb.2010.01.020

Nguyen-Ngoc, T., K. Afshar, and P. Gönczy. 2007. Coupling of cortical dynein and G alpha proteins mediates spindle positioning in *Caenorhabditis elegans*. *Nat. Cell Biol.* 9:1294–1302. http://dx.doi.org/10.1038/ncb1649

Quann, E.J., E. Merino, T. Furuta, and M. Huse. 2009. Localized diacylglycerol drives the polarization of the microtubule-organizing center in T cells. *Nat. Immunol.* 10:627–635. http://dx.doi.org/10.1038/ni.1734

Quann, E.J., X. Liu, G. Altan-Bonnet, and M. Huse. 2011. A cascade of protein kinase C isozymes promotes cytoskeletal polarization in T cells. *Nat. Immunol.* 12:647–654. http://dx.doi.org/10.1038/ni.2033

Redemann, S., J. Pecreaux, N.W. Goehring, K. Khairy, E.H. Stelzer, A.A. Hyman, and J. Howard. 2010. Membrane invaginations reveal cortical sites that pull on mitotic spindles in one-cell *C. elegans* embryos. *PLoS ONE*. 5:e12301. http://dx.doi.org/10.1371/journal.pone.0012301

Singleton, K., N. Parvaze, K.R. Dama, K.S. Chen, P. Jennings, B. Purtic, M.D. Sjaastad, C. Gilpin, M.M. Davis, and C. Wülfing. 2006. A large T cell invagination with CD2 enrichment resets receptor engagement in the immunological synapse. *J. Immunol.* 177:4402–4413.

Spector, D.L., R.D. Goldman, and L.A. Leinwand. 1998. Cells: a laboratory manual. Cold Spring Harbor Laboratory Press, Cold Spring Harbor, NY.

Stinchcombe, J.C., E. Majorovits, G. Bossi, S. Fuller, and G.M. Griffiths. 2006. Centrosome polarization delivers secretory granules to the immunological synapse. *Nature*. 443:462–465. http://dx.doi.org/10.1038/nature05071

Ten Hoopen, R., C. Cepeda-García, R. Fernández-Arruti, M.A. Juanes, N. Delgehyr, and M. Segal. 2012. Mechanism for astral microtubule capture by cortical Bud6p priming spindle polarity in *S. cerevisiae*. *Curr. Biol.* 22:1075–1083. http://dx.doi.org/10.1016/j.cub.2012.04.059

Tsun, A., I. Qureshi, J.C. Stinchcombe, M.R. Jenkins, M. de la Roche, J. Kleczkowska, R. Zamoyska, and G.M. Griffiths. 2011. Centrosome docking at the immunological synapse is controlled by Lck signaling. *J. Cell Biol.* 192:663–674. http://dx.doi.org/10.1083/jcb.201008140

Vallee, R.B., R.J. McKenney, and K.M. Ori-McKenney. 2012. Multiple modes of cytoplasmic dynein regulation. *Nat. Cell Biol.* 14:224–230. http://dx.doi.org/10.1038/ncb2420

Wu, X., X. Xiang, and J.A. Hammer III. 2006. Motor proteins at the microtubule plus-end. *Trends Cell Biol.* 16:135–143. http://dx.doi.org/10.1016/j.tcb.2006.01.004

Yi, J., X.S. Wu, T. Crites, and J.A. Hammer III. 2012. Actin retrograde flow and actomyosin II arc contraction drive receptor cluster dynamics at the immunological synapse in Jurkat T cells. *Mol. Biol. Cell*. 23:834–852. http://dx.doi.org/10.1091/mbc.E11-08-0731